Journal of Asian Concrete Federation
Vol. 2, No. 1, pp. 67-80, June 2016
ISSN 2465-7964 / eISSN 2465-7972
http://dx.doi.org/10.18702/acf.2016.06.2.1.67

Direct-tensile and flexural strength and toughness of high-strength fiber-reinforced cement composites with different steel fibers

Seongwoo Gwon and Myoungsu Shin*

(Received: February 20, 2016; Accepted: May 1, 2016; Published online: July 05, 2016)

Abstract: The main purpose of this study is to investigate effects of the type and volume fraction of steel fibers on the mechanical behaviors of fiber-reinforced cement composites (FRCCs) with high strengths. Various FRCC mix cases were designed and tested in two steps. At the 1st step, two types of steel fibers (straight and hooked) were examined with two different fiber volumes (1.0 and 1.5%). The test variables of the 1st step included the type and volume fraction of steel fibers, and the inclusion of coarse aggregate. At the 2nd step, ultrahigh strength FRCC mix cases using hooked steel fibers only were tested with two different fiber volumes (1.0 and 1.5%). Various mechanical tests were performed to evaluate the stress-strain behaviors of the FRCCs subjected to uniaxial compression, direct tension, and third-point bending. The test results reveal that the use of hooked steel fibers improved the tensile and flexural capacities of FRCCs more effectively than did the straight steel fibers. Also, the FRCCs generally demonstrated greater direct-tensile and flexural toughness compared with ordinary fiber reinforced concretes (FRCs).

Keywords: steel fiber, fiber reinforced cement composites, mechanical strength, strain-hardening behavior, toughness.

1. Introduction and background

High-performance fiber-reinforced cement composites (HPFRCCs), originally defined by Naaman [1], typically consist of cement, water, fibers (such as synthetic, steel, or natural), fine aggregate, and super plasticizer. HPFRCCs demonstrate significant potentials toward the resilience and sustainability of urban infrastructure. In the early years, the development of HPFRCCs has aimed at mitigating the brittle failure of concrete under severe loading and ensuring the long-term integrity of concrete [2-5]. Due to the quasi-brittle characteristics and low tensile strength of concrete, reinforced concrete structures often need considerable transverse reinforcement. This conventional method may cause not only reinforcement congestion but also construction cost burden in critical shear or moment zones.

HPFRCCs are characterized to exhibit large deformation capacity in tension by developing strain hardening through consecutive fiber pullout and bridging over multiple micro-cracks, while FRCs undergo strain softening behavior just after the onset of first cracking (Fig. 1). In an HPFRCC, tensile stresses are transferred between cracks via fiber bridging. Typical features of normal concrete (NC), FRC, and HPFRCC are characterized by the tensile stress-strain relationships up to failure (Fig. 1) [6,7]. HPFRCCs provide not only excellent ductility in both tension and compression, but also higher energy dissipation [4,8]. Moreover, HPFRCCs are also effective in enhancing the shear strength, displacement capacity, and damage tolerance of structural members.

Despite the aforementioned advantages, HPFRCCs raise several critical issues that impede their practical applications in the construction field. Most of all, little research has been conducted to resolve the high material cost issue of HPFRCCs, compared with conventional concrete [9,10]. To the authors' discretion, it is essential to develop low-cost FRCCs exhibiting adequate performances with inexpensive types of fibers [11]. In addition, further research is needed to evaluate the effectiveness of FRCCs in ultra-high strength applications as higher strength cement-based materials generally undergo more brittle behavior [12-14].

Given the concerns, the main objective of this study was to investigate effects of the type and vol-

Corresponding author Myoungsu Shin is a Professor of the Urban and Environmental Engineering, Ulsan National Institute of Science and Technology, Ulsan, Republic of Korea.
Seongwoo Gwon is a Ph.D. student of Urban and Environmental Engineering, Ulsan National Institute of Science and Technology (UNIST), Ulsan, Korea.

ume fraction of steel fibers on the mechanical behaviors of high strength FRCCs. The main test variables were the type and volume fraction of steel fibers, the inclusion of coarse aggregate, water-to-binder ratio, and the type of micro filler. The stress-strain behaviors of the FRCCs were evaluated subjected to uniaxial compression, direct tension, and third-point bending. This study also examined one traditional type of the FRCCs with coarse aggregate typically called "FRC" to set the basis for the cost effectiveness of the other FRCCs.

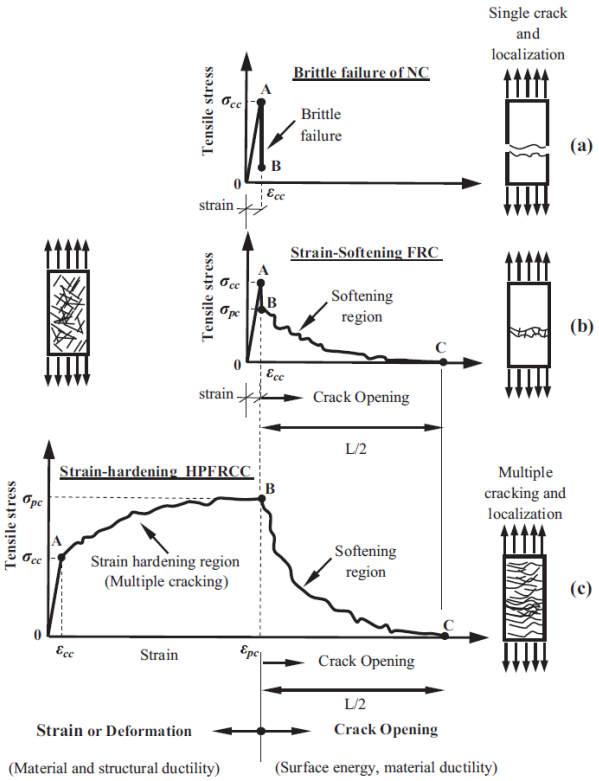

Fig. 1 – Typical stress-strain curves in tension: (a) normal concrete (NC); (b) fiber-reinforced concrete (FRC); and (c) high performance fiber-reinforced cementitous composites (HPFRCC) [6,7]

2. Experimental program

In this section, the material mix designs and test methods used to investigate the mechanical behaviors of various FRCCs are described. A total of five FRCC cases was designed and tested in two steps by varying the proportions of ingredients and the type and volume fraction of steel fibers. Two types of steel fibers were used: hooked fibers manufactured by Bekaert [15] and straight fibers imported from China (see Fig. 2). The detailed information of the steel fibers is summarized in Table 1. All specimens were cured in a controlled curing machine at a humidity of 60% and a temperature of 40 ℃ during 7 days after casting. The load-deformation responses of the FRCCs were acquired by conducting uniaxial compression, direct tension, and third-point bending tests.

(a) hooked fibers (b) straight fibers

Fig. 2 – Hooked and straight steel fibers

Table 1 – Physical properties of steel fibers

Type	Length (mm)	Diameter (mm)	Aspect ratio (L/D)	Tensile strength (MPa)
Straight	25	0.40	60	1,000
Hooked	30	0.38	80	2,300

2.1 First step mix design

Three FRCC mix cases were designed in the 1st step, of which the detailed compositions are presented in Table 2. In naming a case code, the first number "1" or "2" means the test step, and the following two characters stand for the type of steel fibers, "SF" for straight fibers and "HF" for hooked fibers. The number next to them means the volume fraction of steel fibers, "10" for 1.0% and "15" for 1.5%. The last character indicates the existence of coarse aggregate, "Y" for presence and "N" for absence.

Among the mix cases, 1HF10Y and 1SF15Y differed from each other only by the type and volume fraction of steel fibers; 1HF10Y and 1SF15Y contained 1.0% hooked fibers and 1.5% straight fibers, respectively. The two mix cases included natural coarse aggregate with the maximum size of 10 mm, and were made with identical proportions of ingredients, i.e., the same water-to-binder ratio of 28.8% and fine aggregate ratio of 60%. In contrast, 1HF15N with 1.5% hooked fibers included no coarse aggregate (fine aggregate ratio of 100%), and it contained a higher binder content and thus a lower water-to-binder ratio of 24.6%, compared to those of 1HF10Y and 1SF15Y.

2.2 Second step mix design

In the 2nd step, two FRCC mix cases using only hooked steel fibers were tested: 2HF10Y and 2HF15N (see Table 2). The hooked fibers were included at two different volume fractions of 1.0% and 1.5% in 2HF10Y and 2HF15N, respectively.

The only difference in the components of the 2nd step was ground granulated blast furnace slag (GGBFS); fly ash was used instead of GGBFS in the 1st-step mix cases. The 2nd-step mix cases had lower water-to-binder ratios than the 1st-step mix cases; 2HF10Y and 2HF15N had water-to-binder ratios of 24.0% and 24.6%, respectively. 2HF10Y included the same coarse aggregate as in 1HF10Y and 1SF15Y, while 2HF15N included no coarse aggregate.

Table 2 – Mix proportions of tested FRCCs

Case code		1HF10Y	1SF15Y	1HF15N	2HF10Y	2HF15N
Maximum size of coarse aggregate (mm)		10	10	-	10	-
Slump (mm)		-	80 ~ 90	-	-	-
Air content (%)		4	4	4	4	4
Water/binder ratio (wt. %)		28.8	28.8	24.6	24.0	24.6
Sand/aggregate ratio (vol. %)		60	60	100	60	100
Fiber fraction (vol. %)		1.0	1.5	1.5	1.0	1.5
Ingredient contents (kg/m^3)	Water	223	222	239	238	241
	Cement	543	540	817	795	784
	Fly ash or GGBFS	194 (fly ash)	193 (fly ash)	117 (fly ash)	139 (GGBFS)	137 (GGBFS)
	Silica fume	39	39	39	60	59
	Sand	699	695	972	596	981
	Gravel	466	463	-	397	-
	Superplasticizer	2.7	2.7	3.9	3.38	4.34
	HPMC[1]	0.4	0.4	0.2	0.2	0.2

Note: 1. HPMC is Hypromellose used as a viscosity modifying agent.

2.3 Test methods

2.3.1 Compression and elastic modulus tests

The compression tests complied with ASTM C39 [16]. Cylindrical specimens with 100 mm in diameter and 200 mm in length were manufactured and tested. The top and bottom faces of every specimen were adequately grinded and equipped with neoprene pad caps (ASTM C1231 [17]) to enable a uniform stress distribution. Three extensometers with a gauge length of 100 mm were installed around the perimeter of the specimen to measure the longitudinal strain (Fig. 3). The average of the three values was taken as the compressive strain in the specimen. The modulus of elasticity of each specimen is estimated using the compressive stress-strain curve, taken equal to the slope of the secant line between the origin and the point at 40% of the maximum compressive stress [12]. The tests were displacement-controlled at a loading rate of 0.5 mm/min.

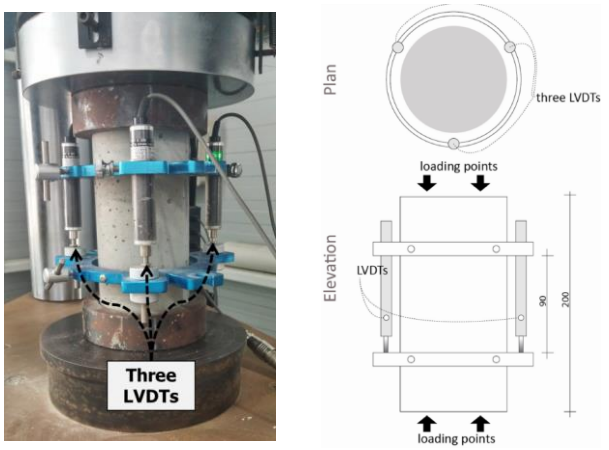

Fig. 3 – Compression test setup (unit: mm)

2.3.2 Flexure test

The flexure tests were performed following ASTM C1609 [18], "Standard test method for flexural performance of fiber-reinforced concrete (using beam with third-point loading)". 400 mm-long prismatic beam specimens with a 100 mm × 100 mm cross-section were loaded in third-point bending. At least three specimens were tested in bending for each mix case. To measure the deflection of the specimen at midspan, two linear variable differential transformers (LVDTs) with a gauge length of 100 mm were installed at the front and rear faces of the specimen using a steel fixture (see Fig. 4). The average of the two values was taken as the deflection of the beam specimen. The purpose of using the LVDT-mounting fixture was to avoid reading deformations due to the settlement or twisting of the beam at the supports [18,19]. The loading was displacement-controlled at different rates in two separate phases: up to the net deflection equal

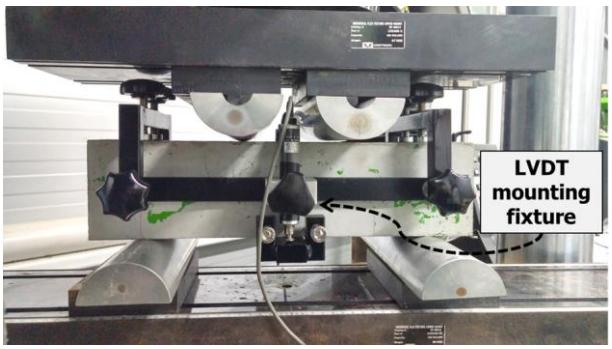

(a) Front view

(b) Side view

Fig. 4 – Third-point bending test setup

to the span length (300 mm) divided by 900, the loading rate was 0.025 mm/min, and beyond that deflection, the loading rate was increased to 0.05 mm/min.

2.3.3 Direct tension test

Dog-bone-shaped specimens were used for the direct tension tests. The specimen dimensions and the test setup are shown in Fig. 5. This test configuration is similar to that used by the research group at the University of Michigan [20]. At least three specimens for each mix case were tested in direction tension. Two extensometers with a gauge length of 178 mm were installed at the sides of the specimen (Fig. 5), aligned with the loading direction, to measure the longitudinal strain. The average of the two values was taken as the tensile strain in the specimen. Two layers of steel wire mesh were embedded at each end of the dog-bone specimen to avoid failure occurring outside the gauge length. The direct tension tests were displacement-controlled at a loading rate of 0.5 mm/min based on the JSCE recommendation [21].

3. Test results and discussions

In this section, the test results are presented and discussed. In particular, the compressive strength, modulus of elasticity, direct tensile strength and ductility, and flexural strength and toughness are compared among the FRCC mix cases.

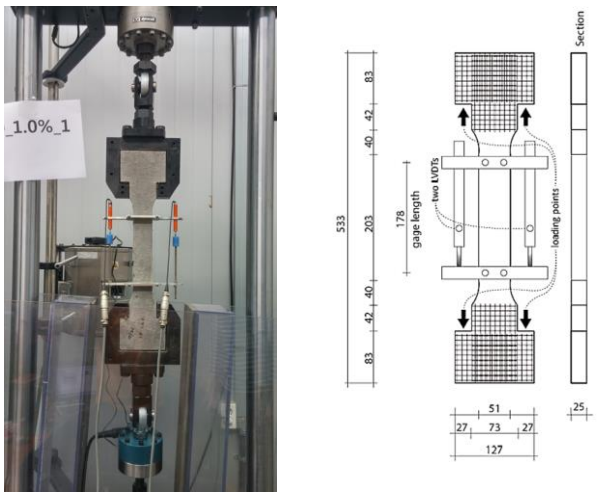

Fig. 5 – Dog-bone specimen configuration for direct tensile tests (unit: mm)

3.1 Compressive strength and modulus of elasticity

Figure 6 shows the compressive stress-strain responses of the three FRCC cases in the 1st step. The compressive strengths and moduli of elasticity are summarized in Table 3. The compressive stress-strain response of every specimen presented no softening curve after reaching the maximum stress, which was due to a brittle failure mechanism that is typical in high strength concrete.

It has been generally reported that there is no considerable effect of steel fibers on the compressive strength development of FRCCs. However, the use of 1.5% straight fibers (1SF15Y) induced a 10.7% higher compressive strength than 1HF10Y. Since there is no difference in the mix proportions between 1SF15Y and 1HF10Y except the fiber type and amount (see Table 2), it is concluded that the 5% higher volume fraction of steel fibers resulted in a greater compressive strength. 1HF15N achieved the highest compressive strength among the three cases. 1HF15N showed about a 37.3% higher compressive strength than 1HF10Y. This was likely attributed to combined effects of a higher ratio (1.5%) of hooked fibers and a higher cement content among the three cases (see Table 2).

The elastic moduli of the 1st step FRCCs (E_{fc}), determined from the measured compressive stress-strain curves, are presented in Table 3. The three mix cases exhibited similar elastic modulus values of approximately 23.6 to 26.6 GPa. The elastic modulus of concrete is known to be generally proportional to the compressive strength. To compare

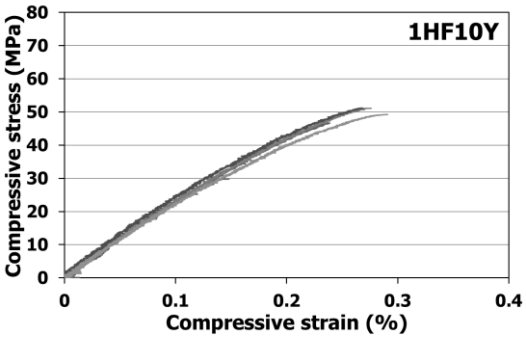

(a)

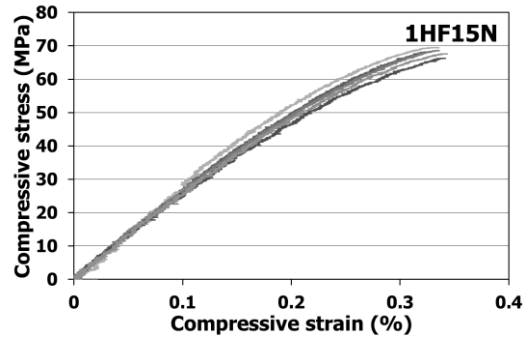

(b)

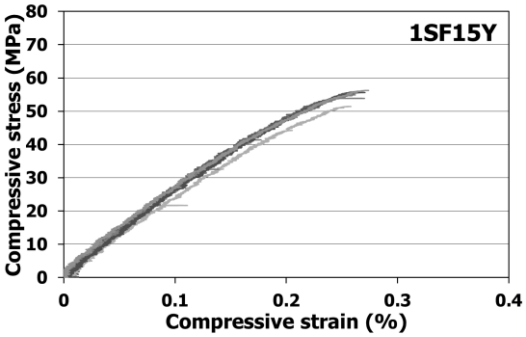

(c)

Fig. 6 – Compressive stress-strain curves of the 1st step FRCCs

the elastic moduli of the tested FRCCs with Portland cement concretes, the elastic modulus of an ordinary Portland cement concrete (E_{cc}) having the same strength as each FRCC is calculated per Neville.

$$E_{cc} = 4730\sqrt{f_{c,max}} \quad (1)$$

where, $f_{c,max}$ is the compressive strength of concrete.

The E_{fc}-to-E_{cc} ratios in Table 3 suggest that the elastic moduli of the 1st step FRCCs were on average about 28.5% smaller than those of Portland cement concretes. In particular, 1HF15N with a higher content of steel fibers and no coarse aggregate showed the smallest E_{fc}-to-E_{cc} ratio. Also, the strain at $f_{c,max}$ ranges from 0.0027 to 0.0034, which are slightly larger than those of Portland cement concretes with similar strengths. The strain at the peak stress was the largest in the case with a higher content of fibers and no coarse aggregate, 1HF15N.

It was reported that the increase of fiber content usually enhanced the modulus of elasticity. However, 1SF15Y and 1HF10Y, both having coarse aggregate, showed similar elastic modulus (E_{fc}) values, although 1SF15Y contained 5% more steel fibers. Therefore, it is deemed that the straight fibers were poorer than the hooked fibers at developing the stiffness. Figure 7 illustrates the compressive stress-strain responses of the two FRCC cases in the 2nd step, and the compressive strengths and moduli of elasticity are given in Table 4. All specimens of the 2nd step tests also showed no softening curve after reaching the maximum stress because of brittle failure. In general, the 2nd-step mix cases achieved much higher compressive strengths than the 1st-step mix cases. The average compressive strengths of 2HF10Y and 2HF15N were 93.3 MPa and 92.5 MPa, respectively. Even though only a single type of steel fibers were used in the 2nd step, it was difficult to distinguish the effect of fiber fraction on the compressive strength due to multiple variables in the mixture proportions. It was likely that the use of GGBFS instead of fly ash, as well as a higher content of silica fume, greatly affected the higher strength development in the 2nd-step mix cases.

Table 3 – Compressive strengths and moduli of elasticity of 1st step FRCCs

Case code	Compressive strength (MPa)		Strain at maximum compressive stress		Elastic modulus, E_{fc} (GPa)		[1]E_{cc} (GPa)	E_{fc}/E_{cc} (%)
	Average	Standard dev.	Average	Standard dev.	Average	Standard dev.		
1HF10Y	49.5	2.1	0.0027	0.0002	23.6	1.1	33.0	71.5
1SF15Y	54.9	2.0	0.0027	0.0001	26.6	2.0	35.0	75.9
1HF15N	68.1	1.2	0.0034	0.0001	26.2	0.4	39.0	67.1

Note: 1. $E_{cc} = 4730\sqrt{f'_{c,max}}$

Table 4 – Compressive strengths and moduli of elasticity of 2nd step FRCCs

Case code	Compressive strength (MPa)		Strain at maximum compressive stress		Elastic modulus, E_{fc} (GPa)		[1]E_{cc} (GPa)	E_{fc}/E_{cc} (%)
	Average	Standard deviation	Average	Standard deviation	Average	Standard deviation		
2HF10Y	93.6	2.5	0.0027	0.0003	43.8	9.9	45.5	96.3
2HF15N	92.5	3.2	0.0028	0.0001	38.3	0.4	45.5	84.2

Note: 1. $E_{cc} = 4730\sqrt{f'_{c,max}}$

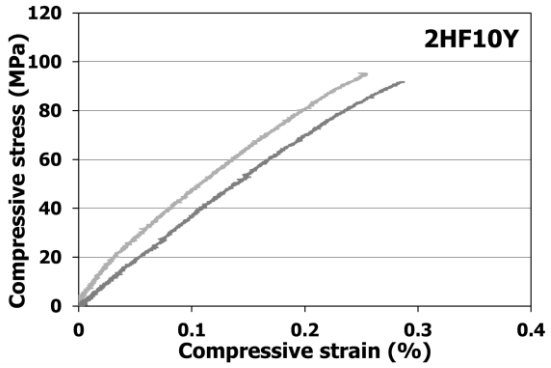

(a)

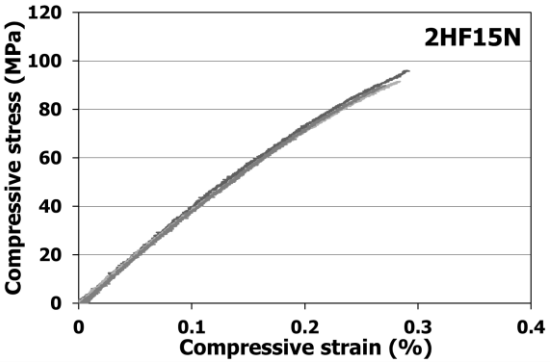

(b)

Fig. 7 – Compressive stress-strain curves of the 1st step FRCCs

The analysis of elastic modulus for the 2nd-step mix cases followed the same procedure as that used for the 1st-step mix cases. The measured elastic moduli (E_{fc}) of the 2nd step FRCCs were much larger than those of the 1st step FRCCs. The larger stiffnesses are in accordance with the higher compressive strengths of the 2nd step FRCCs. 2HF15N showed a 12.6% lower elastic modulus than 2HF10Y. When the FRCCs are compared with Portland cement concretes having similar strengths, the E_{fc}-to-E_{cc} ratios in 2HF10Y and 2HF15N are 0.96 and 0.84, respectively in Table 4. The strain at $f_{c,max}$ ranges from 0.0027 to 0.0028, which are similar to the values observed in the 1st step tests.

The failure modes of all FRCC cases subjected to compression are displayed in Fig. 8. It is clearly

(a) 1HF10Y

(b) 1HF15N

(c) 1SF15Y

(d) 2HF10Y

(e) 2HF15N

Fig. 8 – Failure modes in compression tests

demonstrated that partial crushing or macro cracks were dominant in 1HF10Y, 1SF15Y, and 2HF10Y, while in 1HF15N and 2HF15N, multiple micro-cracks coalesced into macro-cracks that fully developed through the entire specimens. The coalescence of micro-cracks into macro-cracks is likely attributed to no use of coarse aggregate and the higher volume fraction of hooked fibers. Also, the relatively low modulus of elasticity of 1HF15N or 2HF15N in each step is primarily due to these mixing conditions, showing good agreement with both larger strain capacity and less stress concentration through the matrix. The E_{fc}-to-E_{cc} ratio was 67.1% for 1HF15N, smaller than 71.5% and 75.9% for 1HF10Y and 1SF15Y respectively in Table 3, and the E_{fc}-to-E_{cc} ratio was 84.2% for 2HF15N, smaller than that of 2HF10Y in Table 4.

3.2 Flexural strength and toughness

Figure 9 shows the load-deflection responses of the 1st step FRCCs, which present the flexural stress at the bottom of the beam versus the deflection measured by the two LVDTs at midspan. A summary of the test results is given in Table 5. In each test, micro-cracks started to develop when the flexural stress reached the cracking point, from which the load-deflection curve became nonlinear (see Fig. 9). Until the end of testing, micro-cracks sensible by the naked eye were all positioned at the tension zone of the specimen. The failure of each specimen occurred when a couple of cracks at midspan suddenly got widened as shown in Fig. 10.

Among the three cases in the 1st step, 1HF15N achieved the highest flexural strength with an average of 14.5 MPa, while 1SF15Y showed the lowest strength of 7.7 MPa. Also, 1HF10Y with 1.0% fiber ratio had a higher flexural strength than 1SF15Y with 1.5% fiber ratio, which implies that the hooked fibers were more effective in the flexural strength development than the straight fibers (Note that 1HF10Y had a lower compressive strength than 1SF15Y). Therefore, it is deemed that the fiber type as well as the higher fiber ratio in 1HF15N contributed to the development of the highest flexural strength.

Up to the maximum load, 1HF15N developed steady deflection hardening behavior, and had a deflection of 1.27 mm at the peak stress, which was the largest in the 1st-step mix cases. It was observed that the hooked fibers provided favored cracking bridging effects in 1HF15N (see Fig. 10). Overall, the superior flexural behavior of 1HF15N was likely due to combined effects of the higher ratio of hooked fibers and no use of coarse aggregate.

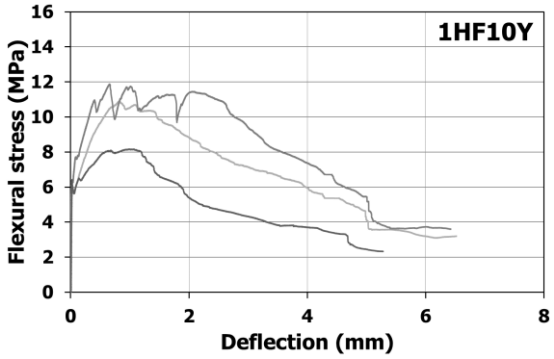

(a)

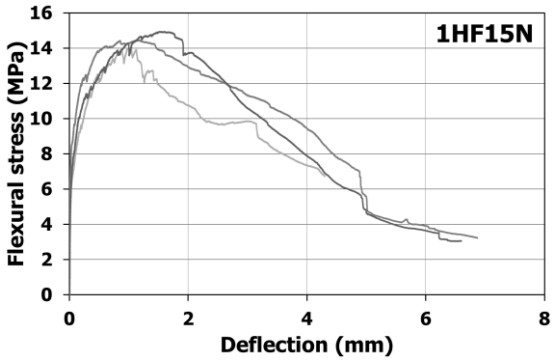

(b)

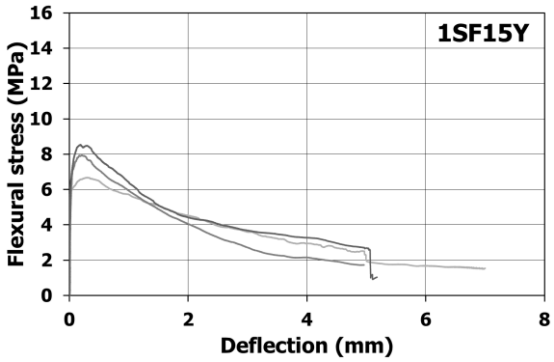

(c)

Fig. 9 – Flexural stress-deflection curves of the 1st step FRCCs

1HF10Y also showed deflection hardening behavior, although the behavior was less consistent than that of 1HF15N in Fig. 9. In contrast, 1SF15Y showed the least ductility with no deflection hardening in Fig. 9, even though it contained a higher volume fraction of steel fibers than 1HF10Y. It also showed the least deflection of 0.23 mm at the peak stress. The results suggest that the hooked fibers provided better crack bridging effects than the straight fibers (see Fig. 10). After reaching the peak stress, 1SF15Y displayed a rapid deflection softening response contrary to the other cases.

Table 5 – Summary of flexural strengths and deflections

Case code	First peak stress, f_1 (MPa)		Deflection at f_1, δ_1 (mm)		Flexural strength, f_p (MPa)		Deflection at f_p, δ_p (mm)	
	Average	Standard dev.	Average	Standard dev.	Average	Standard dev.	Average	Standard dev.
1HF10Y	6.3	0.1	0.02	0.01	10.3	1.9	0.85	0.21
1SF15Y	7.7	0.9	0.23	0.07	7.7	0.9	0.23	0.07
1HF15N	11.8	0.6	0.31	0.02	14.5	0.5	1.27	0.29
2HF10Y	11.5	1.5	0.34	0.11	13.3	1.4	0.74	0.28
2HF15N	12.1	1.0	0.18	0.10	18.4	2.3	0.98	0.15

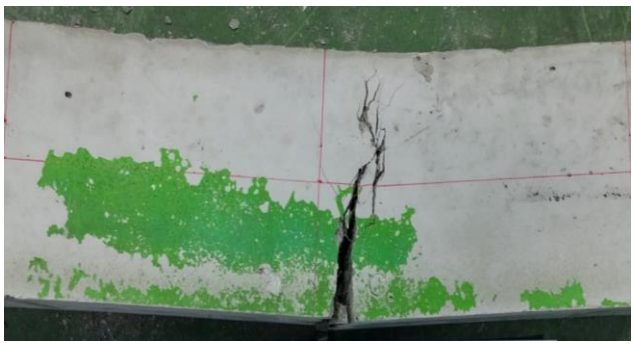

(a) 1HF10Y

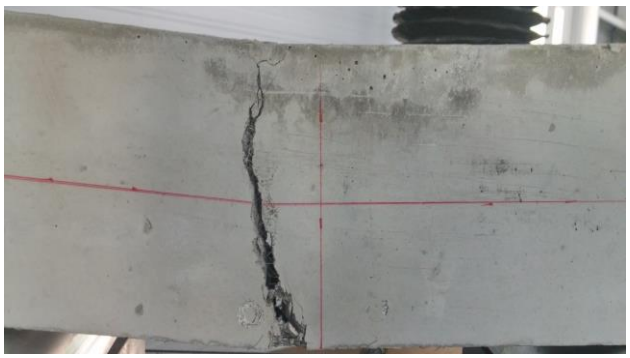

(b) 1SF15Y

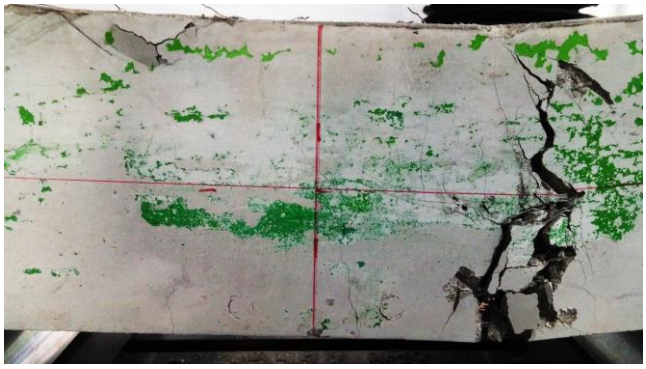

(c) 1HF15N

Fig. 10 – Failure modes of the 1st step FRCCs in flexural tests

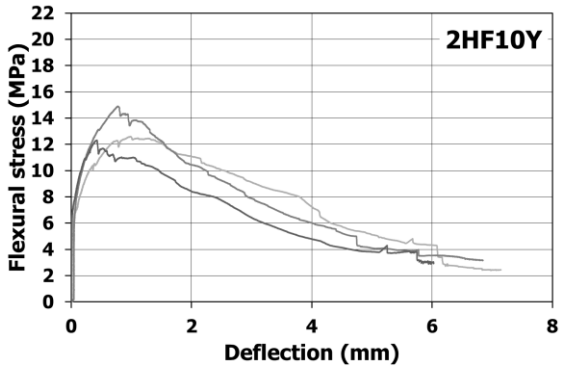

(a)

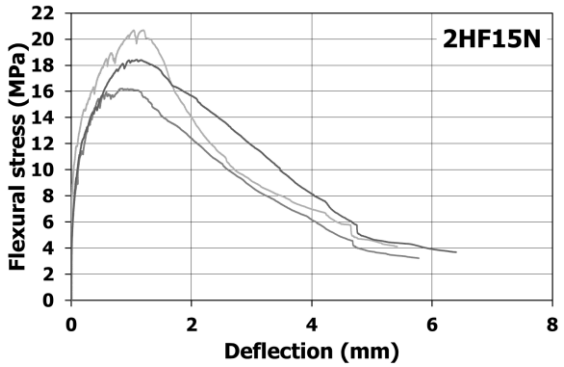

(b)

Fig. 11 – Flexural stress-deflection curves of the 2nd step FRCCs

2HF15N achieved higher flexural strengths than the 1st-step mix cases in Table 5. As discussed earlier, the different type of micro filler and silica fume ratio could also affect the flexural performance. However, 2HF10Y and 2HF15N showed less ductile load-deflection behaviors than 1HF10Y and 1HF15N (see Fig. 11). The deflections at the peak stress in 2HF10Y and 2HF15N are 0.74 mm and 0.98 mm, respectively, smaller than those in 1HF10Y and 1HF15N in Table 5. Between 2HF10Y and 2HF15N, the deflection at the peak stress was higher in 2HF15N with a larger amount of fibers and no coarse aggregate, as observed in the 1st step. The load-deflection curve began to be non-

linear at a flexural stress of about 8.0 MPa and 11.0 MPa in 2HF10Y and 2HF15N, respectively. These values are greater than those in the 1st-step mix cases.

Figures 10 and 12 present the cracking damages after the failures of the beam specimens. All the tests continued until a sudden collapse occurred. The photographs of the specimens were taken at the end of testing. In the 1st step (see Fig. 10), multiple cracks developed at the tension zone and propagated in a relatively irregular path in the two cases with hooked fibers. However, 1SF15Y showed a single large crack opening near the midspan. 1SF15Y showed the least number of cracks among the 1st-step mix cases, while 1HF15N developed the greatest number of micro-cracks. In the 2nd step (see Fig. 12), 2HF15N with hooked fibers showed diagonal cracks across the centerline at which many micro-cracks coalesced.

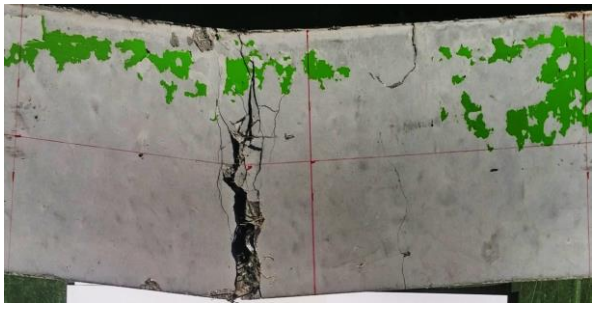

(a) 2HF10Y

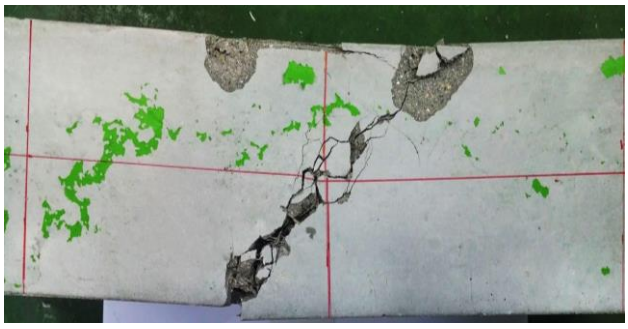

(b) 2HF15N

Fig. 12 – Failure modes of the 2nd step FRCCs in flexural tests

In a load-deflection response from a third-point bending test, the modulus of rupture is obtained using the following:

$$f = \frac{PL}{bh^2} \tag{2}$$

where P is the applied load, L is the span length (300 mm in this study), and b and h are the width and depth of the prismatic beam specimen, respectively. According to ASTM C1609, the first-peak strength (f_1) and the residual strengths (f_{150}^D and f_{600}^D) at the deflections of L/150 and L/600 can be estimated by:

$$f_1 = \frac{P_1 L}{bh^2} \tag{3}$$

$$f_{150}^D = \frac{P_{150}^D L}{bh^2}, \qquad f_{600}^D = \frac{P_{600}^D L}{bh^2} \tag{4}$$

where P_1 is the first-peak load corresponding to the first local maximum at which generally the initial cracking occurs, and P_{150}^D and P_{600}^D are the residual loads at the deflections of L/150 and L/600 after cracking, respectively. The first-peak strength (f_1) signifies the flexural behavior of fiber-reinforced concrete up to the onset of first cracking, and the residual strengths (f_{150}^D and f_{600}^D) characterize the residual capacity after cracking.

The toughness of a specimen at the deflection of L/150 (T_{150}^D) is a measure of the energy absorption capacity of the material. In other words, the toughness is an index for the material's capability to absorb energy and deform plastically without fracturing. The toughness is quantified as the area under the load-deflection curve at a certain deflection level. Then, the equivalent flexural strength ratio ($R_{T,150}^D$) can be determined by:

$$R_{T,150}^D \ (\%) = \frac{150 T_{150}^D}{f_1 bh^2} \times 100 \tag{5}$$

where $R_{T,150}^D$ is a dimensionless parameter signifying the relative magnitude of the residual strength (f_{150}^D) at the deflection of L/150 with respect to the first-peak strength (f_1). Refer to Fig. 13 for the definitions of the aforesaid parameters.

For a quantitative evaluation on the flexural behaviors of the FRCC cases, the toughness and equivalent strength ratio are calculated at the deflection of L/150, which is 2 mm in this study. These performance indices are summarized in Table 6. 1SF15Y showed the smallest toughness T_{150}^D of 39.8 kN·mm on average, which indicates poorer energy absorption ability with the straight fibers. In general, the higher fiber volume ratio improved the toughness. The highest toughness of 105.6 kN·mm is obtained in 2HF15N that developed the highest flexural strength and a relatively steady strain-

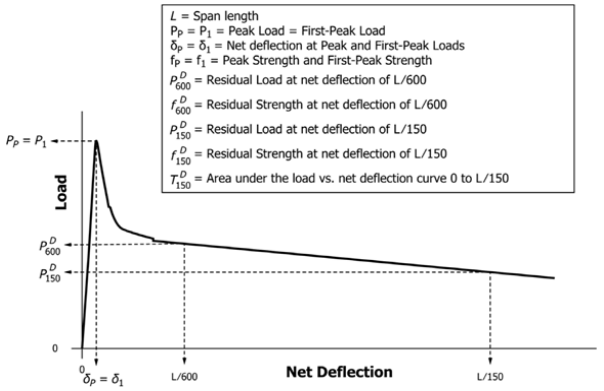

(a) First peak equal to peak load

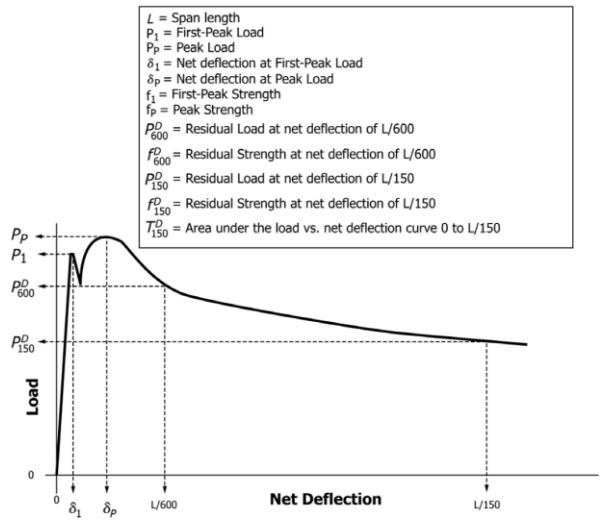

(b) Peak load is greater than first-peak load

Fig. 13 – Key parameters in flexural stress-deflection relationship [16]

hardening behavior due to the better bond between the hooked fibers and matrix.

The equivalent strength ratio ($R^D_{T,150}$) can be interpreted as how the residual strength (f^D_{150}) at the deflection of *L*/150 is compared with the first-peak strength (f_1). The smallest $R^D_{T,150}$ value is for 1SF15Y, as it showed the smallest toughness, while the largest $R^D_{T,150}$ value is for 1HF10Y. Although 2HF15N achieved the greatest toughness, it has a lower equivalent strength ratio than 1HF10Y. This is due to the magnitude of the first-peak strength (f_1); 12.1 MPa for 2HF15N, and 6.30 MPa for 1HF10Y. Considering both the toughness and equivalent strength ratio, it is concluded that 2HF15N showed the best flexural performance in this study.

3.3 Direct tensile strength and ductility

The direct tensile stress-strain responses of the three FRCCs in the 1st step are shown in Fig. 14, and the results are summarized in Table 7. In general, the response of normal concrete is brittle under tension where the response is almost linear elastic up to the onset of first cracking, followed by a sudden decrease in the tensile stress. In contrast, FRCCs generally exhibit better ductility than normal concrete. The inclusion of engineered fibers can change the response after the first cracking. Beyond the peak stress, the tensile stress decreases in a much slower rate due to the bridging action of the fibers developed across multiple micro-cracks.

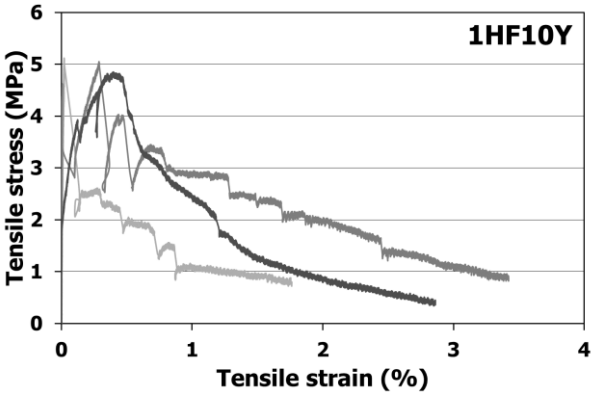

(a)

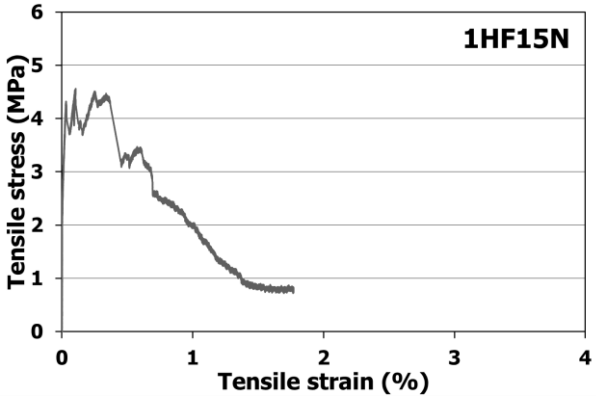

(b)

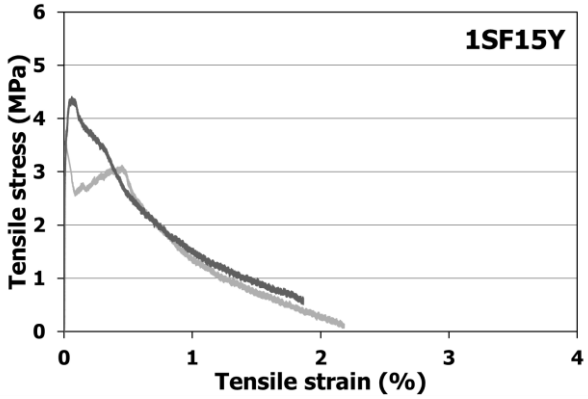

(c)

Fig. 14 – Direct tensile stress-strain curves of the 1st step FRCCs

Table 6 – Toughness index according to ASTM C1609

Case	No.	P^D_{600} (kN)	f^D_{600} (MPa)	P^D_{150} (kN)	f^D_{150} (MPa)	T^D_{150} (kN-mm)	$R^D_{T,150}$ (%)
1HF10Y	1	32.3	9.70	29.3	8.78	63.2	154.5
	2	36.4	10.91	38.0	11.40	70.3	165.3
	3	26.1	7.84	18.0	5.39	47.4	111.3
	Average	31.6	9.48	28.4	8.52	60.3	143.7
	St. dev.	5.2	1.55	10.0	3.01	11.7	28.6
1SF15Y	1	21.6	6.47	15.1	4.53	37.5	84.0
	2	23.8	7.13	13.5	4.05	39.4	74.3
	3	25.9	7.78	14.8	4.43	42.5	74.8
	Average	23.7	7.12	14.5	4.34	39.8	77.7
	St. dev.	2.2	0.66	0.9	0.26	2.5	5.5
1HF15N	1	40.4	12.12	35.9	10.78	78.9	103.1
	2	46.2	13.87	43.0	12.90	89.2	107.8
	3	41.8	12.54	45.6	13.67	87.9	115.6
	Average	42.8	12.84	41.5	12.45	85.3	108.8
	St. dev.	3.0	0.91	5.0	1.50	5.6	6.3
2HF10Y	1	37.0	11.09	37.0	11.09	74.7	108.3
	2	44.3	13.29	34.6	10.39	81.1	92.6
	3	38.8	11.63	28.0	8.41	68.5	94.1
	Average	40.0	12.00	33.2	9.96	74.8	98.3
	St. dev.	3.8	1.15	4.6	1.39	6.3	8.7
2HF15N	1	59.0	17.70	46.7	14.02	115.7	147.7
	2	51.0	15.31	41.2	12.37	94.3	123.9
	3	52.1	15.63	52.2	15.67	106.8	121.4
	Average	54.0	16.21	46.7	14.02	105.6	131.0
	St. dev.	4.3	1.30	5.5	1.65	10.8	14.5

Among the 1st-step mix cases, 1HF10Y showed the highest tensile strength of about 4.89 MPa on average, with developing strain hardening behavior through fiber bridging over multiple micro-cracks up to the peak stress. 1HF10Y showed the largest strain at the tensile strength among the 1st-step mix cases. The stress decreased gradually after reaching the peak stress, as one of the cracks opened widely with no development of new cracks (Fig. 15). There were approximately seven micro-cracks observed with the naked eye.

1SF15Y showed the lowest tensile strength of about 3.96 MPa on average among the 1st-step mix cases. Furthermore, it showed an abrupt stress drop after the first cracking (i.e., no multiple cracks were observed). 1SF15Y showed an inferior tensile response than 1HF10Y, even though 1SF15Y contained a higher ratio of steel fibers, and both cases had the same mix proportions. The inferior tensile behavior of 1SF15Y was attributed to the use of straight fibers, which was also reported in the previous literature.

(a) 1HF10Y

(b) 1HF15N

(c) 1SF15Y

Fig. 15 – Failure modes of the 1st FRCC specimens in direct tension tests

1HF15N showed a lower tensile strength than 1HF10Y despite its larger amount of hooked fibers. However, 1HF15N achieved a higher tensile strength and higher strain capacity than 1SF15Y. This must be due to the effect of hooked fibers, as was concluded by previous researchers. The tensile strength of 1HF15N was developed during the strain hardening-softening phase after the elastic range. There were approximately ten micro-cracks observed with the naked eye (Fig. 15).

For the 2nd step, the direct tensile stress-strain responses of the two FRCCs are shown in Fig. 16, and the results are summarized in Table 7. 2HF15N exhibited the highest tensile strength of 6.65 MPa on average in this study. Also, both 2HF10Y and 2HF15N underwent more ductile behaviors with strain hardening than the 1st-step mix cases, and showed much less fluctuations in the strain hardening phases. The improved tensile behaviors were likely attributed to the better bond between the matrix and hooked fibers than in the 1st-step mix cases. The better bond possibly resulted from the type and content of micro fillers and the increased amount of cement.

For the cases of the 2nd step mixes, 2HF15N with a higher fiber ratio and no coarse aggregate presented a superior performance in tension than 2HF10Y with a lower fiber ratio and coarse aggregate. Comparing 2HF15N and 1HF15N with the same water-to-binder ratio, the higher tensile strength of 2HF15N was likely attributed to the use of GGBFS and a higher content of silica fume (see Table 2).

Table 7 – Summary of direct tensile strengths and strains

Case code	Direct tensile strength (MPa)		Strain at maximum stress (%)	
	Average	Standard dev.	Average	Standard dev.
1HF10Y	4.89	0.16	0.24	0.19
1SF15Y	3.96	0.64	0.03	0.03
1HF15N	4.43	1.18	0.11	-
2HF10Y	4.55	0.95	-	-
2HF15N	6.65	0.95	-	-

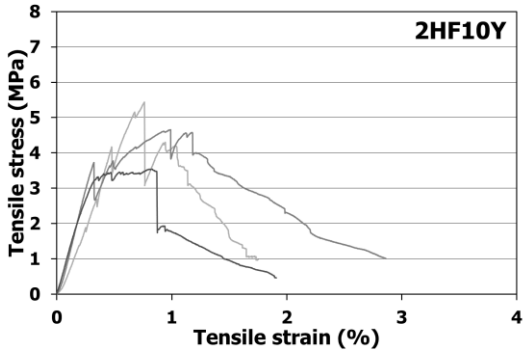

(a)

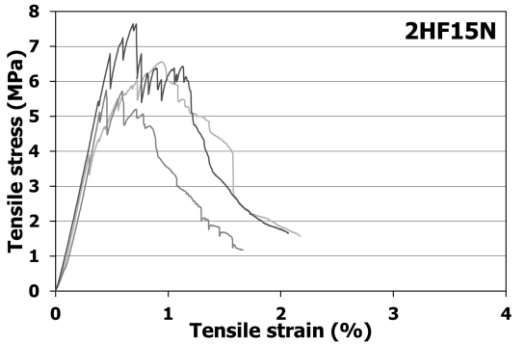

(b)

Fig. 16 – Direct tensile stress-strain curves of the 2nd step FRCCs

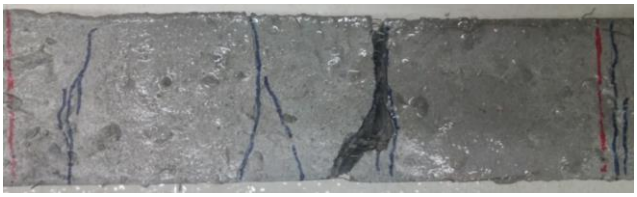

(a) 2HF10Y

(b) 2HF15N

Fig. 17 – Failure modes of the 2nd FRCC specimens in direct tension tests

The cracking damages after the failures of the dog-bone specimens are shown in Fig. 17. All the tests continued until a sudden collapse occurred. The photographs of the specimens were taken at the end of testing. The 2nd-step mix cases gradually developed multiple micro-cracks within the gauge length zone of the LVDTs. As shown in Figs. 15 and 17, the cases with hooked fibers displayed multiple cracks, while only one macro-crack opened

widely in case with straight fibers. Among those with hooked fibers, 1HF15N and 2HF15N with a higher fiber ratio had a larger number of cracks. Comparing the 1st and 2nd step mixes, 2HF15N developed more cracks than 1HF15N. Accordingly, the stress-strain behavior of 2HF15N was superior (see Fig. 16).

4. Conclusions

In this study, five cases of steel fiber-reinforced cement composites (FRCCs) were tested with different types (hooked and straight) and volume fractions (1.0 and 1.5%) of steel fibers, varying the mix proportions (e.g., inclusion of coarse aggregate, types of fillers). Various mechanical tests were conducted, especially focusing on the direct-tensile and flexural behaviors of FRCCs. The findings and conclusions can be summarized as follows:

(1) The compression test results suggest that the hooked fibers were more effective than the straight fibers in developing both the compressive strength and stiffness of FRCCs. Also, a higher volume fraction of steel fibers generally resulted in a greater compressive strength. The use of GGBFS instead of fly ash, as well as a higher ratio of silica fume, greatly improved the compressive strength of FRCCs.

(2) The elastic moduli of the FRCCs were smaller than those of Portland cement concretes with similar strengths. However, the discrepancy was smaller in the ultrahigh strength FRCCs (2nd-step mix cases) than in the high strength FRCCs (1st-step mix cases).

(3) In the direct tension tests, the FRCCs with the hooked fibers developed strain hardening behavior through fiber bridging over multiple micro-cracks. However, the straight fibers did not effectively contribute to both the tensile strength and strain capacity of FRCCs. Also, the ultrahigh strength FRCCs generally exhibited more ductile behaviors, which was likely attributed to the better bond between the steel fibers and matrix including a higher ratio of silica fume as well as GGBFS.

(4) In the flexural tests, the hooked fibers were more effective in the flexural strength development, and provided better crack bridging effects than the straight fibers. The use of straight fibers resulted in an abrupt strength drop, as observed in the direct tension tests. The FRCCs with the higher ratio of hooked fibers and no use of coarse aggregate presented the most favorable flexural behaviors. The ultrahigh strength FRCCs achieved higher flexural strengths, but showed less ductile behaviors than the high strength FRCCs.

(5) From the flexural test results, the higher steel fiber ratio generally improved the toughness. 1SF15Y showed the smallest toughness as well as the smallest equivalent strength ratio, which indicates poorer energy absorption ability with the straight fibers. The highest toughness was obtained in 2HF15N that developed the highest flexural strength and a relatively steady strain-hardening behavior due to the better bond between the hooked fibers and matrix.

Acknowledgements

This research was supported by Global Ph.D. Fellowship Program (NRF-2014H1A2A1020435) through the National Research Foundation of Korea (NRF) funded by the Ministry of Education, as well as Basic Science Research Program (2015R1D1A1A09061167) through the National Research Foundation of Korea (NRF) funded by the Ministry of Education.

References

1. Namman, A.E.; and Reinhardt, H.W. (2006) "Proposed classification of HPFRC composites based on their tensile response," Materials and Structures, 39, pp. 457~555.
2. Wille, K.; Naaman, A.E.; and El-Tawil, S. (2011) "Ultra high performance fiber reinforced concrete," Concrete International, 33(9), pp. 35~41.
3. Kim, D.J.; Naaman, A.E.; and El-Tawil, S. (2009) "High performance fiber reinforced cement composites with innovative slip hardening twisted steel fibers," International Journal of Concrete Structures and Materials, 3(2), pp. 119~126.
4. Li, V. (2003) "On engineered cementitious composites (ECCs); a review of the material and its application," Journal of Advanced Concrete Technology, 1(3), pp. 215~230.
5. Naaman, A.E. (2003) "Engineered steel fibers with optimal properties for reinforcement of cement composites," Journal of Advanced Concrete Technology, 1(3), pp. 241~252.
6. Naaman, A.E.; and Reinhardt, H.W. (1996) "Characterization of high performance fiber reinforced cement composites," HPFRCC, pp. 1~24.
7. Fischer, G.; and Li, V. (2000) "Structural composites with ECC," Proceedings of the ASCCS-6. USC, pp. 1001~1008.
8. Chao, S.; Naaman, A.E.; and Parra-Montesinos, G.J. (2009) "Bond behavior of reinforcing bars in tensile strain-hardening fiber-reinforced cement composites," ACI Structural Journal, 106(6), pp. 897~906.
9. Caballero-Morrison, K.E.; Bonet, J.L.; Navarro-Gregori, J.; and Martí-Vargas, J.R. (2012). "Behaviour of steel-fibre-reinforced normal-strength con-

crete slender columns under cyclic loading," Engineering Structures, 39, pp. 162~175.
10. Lee, H. (2007). "Shear strength and behavior of steel fiber reinforced concrete columns under seismic loading," Engineering Structures, 29(7), pp. 1253~1262.
11. Shin, M.; Choi, Y.Y.; Kim, I.H.; and Lee, K. (2013). "Effectiveness of low-cost fiber-reinforced cement composites in hollow columns under cyclic loading," Construction and Building Materials, 47, pp. 623~635.
12. Mehta, P.K. and Monteiro, P.J.M. (2005) Concrete microstructure, properties, and materials, McGraw-Hill Companies, New York, NY, USA.
13. Doennecke, C. (2003) Softening behavior of ultra-high strength concretes, Technical report, University of Leipzig, German.
14. Shin, M.; Kim, K.; Gwon, S.W.; and Cha, S. (2014) "Durability of sustainable sulfur concrete with fly ash and recycled aggregate against chemical and weathering environments," Construction and Building Materials, 69, pp. 167~176.
15. Dramix® 3D steel fibers for concrete reinforcement, BEKAERT.
16. ASTM International. (2010) ASTM Standard C39: Standard test method for compressive strength of cylindrical concrete specimens, West Conshohocken, PA, USA.
17. ASTM International. (2012) ASTM Standard C1231: Standard practice for use of unbonded caps in determination of compressive strength of hardened concrete cylinders, West Conshohocken, PA, USA.
18. ASTM International. (2010) ASTM C1609/C1609M: Standard test method for flexural performance of fiber-reinforced concrete (using beam with third-point loading).
19. Choi, S.J.; Hong, B.T.; Lee, S.J.; and Won, J.P. (2014) "Shrinkage and corrosion resistance of amorphous metallic-fiber-reinforced cement composites," Composite Structures, 107, pp. 537~543.
20. Sirijaroonchai, K.; El-Tawil, S.; and Parra-Montesinos, G. (2010) "Behavior of high performance fiber reinforced cement composites under multi-axial compressive loading," Cement and Concrete Composites, 32, pp. 62~72.
21. Japan Society of Civil Engineers (JSCE). (2008) Recommendation for design and construction of high performance fiber reinforced cement composite with multiple fine cracks, Concrete Engineering Series 82.
22. Shin, M.; Choi, Y.; Kim, I.; and Lee, K. (2013) "Effectiveness of low-cost fiber-reinforced cement composites in hollow columns under cyclic loading," Construction and Building Materials, 47, pp. 623~635.
23. Shin, M.; Gwon, S.W.; Lee, K.; Han, S.W.; and Jo, Y.W. (2014) "Effectiveness of high performance fiber-reinforced cement composites in slender coupling beams," Construction and Building Materials, 68, pp. 476~490.
24. Neville, A.M. (1997) Properties of concrete, 4th and final ed., Pearson Education, Harlow, UK.
25. De Nicolo, B.; Pani, L.; and Pozzo, E. (1994) "Strain of concrete at peak compressive stress for a wide range of compressive strengths," Materials and Structures, 27(4), pp. 206~210.
26. Qian, X.; Zhou, X.; Mu, B.; and Li, Z. (2003) "Fiber alignment and property direction dependency of FRC extrudate," Cement and Concrete Research, 33(10), pp. 1575~1581.
27. Gul, M.; Bashir, A.; and Naqash, J.A. (2014) "Study of modulus of elasticity of steel fiber reinforced concrete," International Journal of Engineering and Advanced Technology, 3(4), pp. 304~309.
28. Atiş, C.D. and Bilim, C. (2007). "Wet and dry cured compressive strength of concrete containing ground granulated blast-furnace slag," Building and Environment, 42(8), pp. 3060~3065.
29. Turatsinze, A.; Granju, J.L.; and Bonnet, S. (2006) "Positive synergy between steel-fibres and rubber aggregates: effect on the resistance of cement-based mortars to shrinkage cracking," Cement and Concrete Research, 36(9), pp. 1692~1697.
30. Wille, K.; Naaman, A.E.; and Parra-Montesinos, G. (2011) "Ultra high performance concrete with compressive strength exceeding 150 MPa (22ksi): A simpler way," ACI Materials Journal, 108(1), pp. 46~54.
31. Bazant, Z.P. and Planas, J. (1997) Fracture and size effect in concrete and other quasibrittle materials (Vol. 16), CRC press.
32. ACI Committee. (1988). Design Considerations for Steel Fiber Reinforced Concrete (ACI 544.4 R-88), American Concrete Institute.